Results in Engineering 28 (2025) 107905

Contents lists available at ScienceDirect

Results in Engineering

journal homepage: www.sciencedirect.com/journal/results-in-engineering

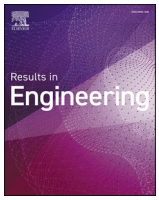

Influence of surface roughness on molecular flow through labyrinth seals for space applications

Josef Pouzar [a,*], David Kostal [a], Lars-Göran Westerberg [b], Erik Nyberg [c], Tomas Polacek [a], Karel Jurik [d], Ivan Krupka [a]

[a] Faculty of Mechanical Engineering, Brno University of Technology, Brno 61669, Czech Republic
[b] Division of Fluid and Experimental Mechanics, Luleå University of Technology, SE-971 87 Luleå, Sweden
[c] Division of Machine Elements, Luleå University of Technology, SE-971 87 Luleå, Sweden
[d] Faculty of Electrical Engineering and Communication, Brno University of Technology, Brno 61600, Czech Republic

ARTICLE INFO

Dataset link: https://doi.org/10.5281/zenodo.15649645

Keywords:
Labyrinth seal
Surface roughness
Transmission probability
Molecular flow
Space mechanisms

ABSTRACT

Labyrinth seals are commonly used in space mechanisms to reduce evaporative losses of lubricant molecules and limit the transport of contaminants. Analytical models and numerical simulations for predicting mass flow through these seals typically assume smooth, idealized surfaces, neglecting the effects of realistic surface roughness. This study systematically investigates the impact of surface roughness on the transmission probability (TP) of oil molecules using Monte Carlo simulations under free molecular flow conditions. Key geometric and surface parameters including average roughness (Ra), corridor length, and seal width are varied to evaluate their influence on molecular transport. The results demonstrate that surface roughness significantly reduces TP and molecular flux, especially in narrow and elongated geometries. Furthermore, increasing surface roughness by an order of magnitude enables a reduction in channel length or an increase in gap width by approximately 35–40 % while maintaining equivalent transmission probability. Based on these findings, a correction model is proposed to improve prediction accuracy and is validated against experimentally measured oil evaporative losses. This work highlights the potential of controlled surface texturing as a design strategy to both enhance sealing effectiveness and enable geometric reductions for improved compactness and manufacturability.

Abbreviations and Symbols

$a(n)$	Wave amplitude [mm]
$A(W, L)$, $B(W, L)$, $C(W, L)$	Polynomial coefficients
$A_{i,j}$, $B_{i,j}$, $C_{i,j}$	Indexed polynomial coefficients
b	Spectral exponent
$f(x)$	Synthetic roughness profile [mm]
g, $g(n)$	Gaussian random function
$h(n)$	Synthetized profile amplitude [mm]
L	Corridor length [mm]
m	Number of data points
n	Spatial frequency
N	Spatial frequency resolution
N_0	Number of molecules entering
N_1	Number of molecules exiting
PC	Parametric curve scaling factor
$PFPE$	Perfluoropolyether
Ra	Arithmetic mean roughness [μm]
Rk	Core roughness depth [μm]
Rku	Kurtosis
Rpk	Reduced peak height [μm]
Rq	Root mean square roughness [μm]
Rsk	Skewness
Rvk	Reduced valley depth [μm]
TP	Transmission probability [-]
u	Uniform random distribution
$u(n)$	Uniform random phase
W	Corridor width [mm]
x	Spatial coordinate [mm]
z	Roughness profile height [mm]
$\bar{z}$	Mean profile height [mm]
z_i	Discrete height value [mm]

* Corresponding author.
E-mail address: Josef.Pouzar@vut.cz (J. Pouzar).

https://doi.org/10.1016/j.rineng.2025.107905
Received 17 October 2025; Accepted 23 October 2025
Available online 24 October 2025

1. Introduction

In space applications, mechanical systems containing liquid lubricants must be sealed to prevent lubricant loss and preserve long-term functionality [1–4]. Non-contact labyrinth seals are widely employed for this purpose, offering a passive means of restricting the migration of lubricant molecules in ultra-high or extreme vacuum environments [5–8]. These seals incorporate a narrow corridor between stationary and rotating components (see Fig. 1), effectively limiting molecular flow without introducing friction or wear [4,7,9]. Preserving lubricant within these systems is critical to ensuring the longevity and reliability of space mechanisms [1,10,11]. The escape and subsequent condensation of evaporated molecules on sensitive surfaces such as optical elements can degrade performance and jeopardize mission success [4,12,13]. These risks underscore the importance of reliable sealing to limit molecular leakage and extend the service life of lubricated systems in space.

Labyrinth seals for space applications may consist of straight channels or more complex geometries [5,6,8]. However, the primary parameters governing molecular flow restriction are the corridor length and width [5,8]. A careful balance between these two parameters is required to ensure mechanical safety while effectively reducing molecular transmission [4,5]. Predicting lubricant evaporative losses can be approached through analytical models or numerical simulations [4,5,7,8]. Both methodologies usually assume smooth internal surfaces with no surface roughness [4,8]. The influence of realistic surface roughness arising from machining [14,15], material processing [16,17], or operational wear [18,19], is neglected despite its potential to alter molecular scattering behaviour and significantly impact transmission probability [20–25]. This effect is particularly important in narrow and elongated seal geometries, where interactions between molecules and surface features are more frequent and cumulative [22,26].

This study investigates the influence of surface roughness on the molecular flow of lubricant through two-dimensional labyrinth seals operating under vacuum conditions. By employing synthetically generated rough surface profiles combined with Monte Carlo simulations, the analysis explores the interaction between roughness parameters and seal geometry, including corridor length and width. The primary outcome is a simulation-based correction model that refines conventional smooth-surface predictions by incorporating realistic surface roughness effects representative of actual labyrinth seals. This model provides a practical and physically grounded tool for predicting lubricant evaporation and highlights the potential to compensate for geometric constraints through surface texturing, enabling possible reductions in seal dimensions without compromising sealing performance.

2. Material and methods

To evaluate the impact of surface roughness on molecular transmission, a numerical model of a straight, two-dimensional labyrinth seal was developed. This geometry, representative of those used in ball bearing systems [4,5], consists of a narrow corridor through which lubricant molecules evaporate and diffuse under vacuum conditions [8,27]. Fig. 1 illustrates the modelled configuration, showing the migration of evaporated molecules along the seal path.

The simulation includes surface roughness on the seal walls to investigate its possible effect on molecular scattering and transmission probability. Synthetic rough profiles were generated using statistical parameters characteristic of real labyrinth seals and integrated into a molecular flow simulation tool. This method enables the tracking of individual molecular trajectories and allows for assessing how surface topography may influence 38 molecular transport through the seal.

2.1. Surface roughness modeling

Simulations were performed using COMSOL Multiphysics 6.3 [28], utilizing the Free Molecular Flow module [29]. Since this module do not natively support surface roughness parameters, surface roughness was instead introduced as a geometric modification of the canal walls in a 2D simulation domain.

A common approach to modelling surface roughness is based on its spatial frequency content, analogous to the Fourier representation of temporal signals [20,30–33]. This approach allows for the synthesis of roughness profiles by summing a finite number of cosine waves with randomized amplitudes and phases. In one spatial dimension, an elementary cosine wave is given by

$$\cos(2\pi(\boldsymbol{nx})) \tag{1}$$

where n is the spatial frequency and x is the spatial coordinate. The synthetic surface roughness profile height z as a function $f(x)$ is synthesized as a discrete superposition of such wave

$$z = f(\boldsymbol{x}) = \sum_{n=-N}^{N} \boldsymbol{a}(\boldsymbol{n})\cos\left(2\pi(\boldsymbol{nx}) + u(n)\right) \tag{2}$$

Here $a(n)$ is wave amplitude, and $u(n)$ is random phase angle drawn from a uniform distribution over the interval $[-\pi/2, \pi/2]$, that cosine term span the full range from –1 to 1. Isotropy is achieved by including both positive and negative frequency components symmetrically ($-N$, N). To reflect realistic surface statistics, the amplitude is computed as

$$a(\boldsymbol{n}) = g(n)\cdot h(\boldsymbol{n}) \tag{3}$$

where

$$h(\boldsymbol{n}) = \frac{1}{(\boldsymbol{n}^2)^{b/2}} \tag{4}$$

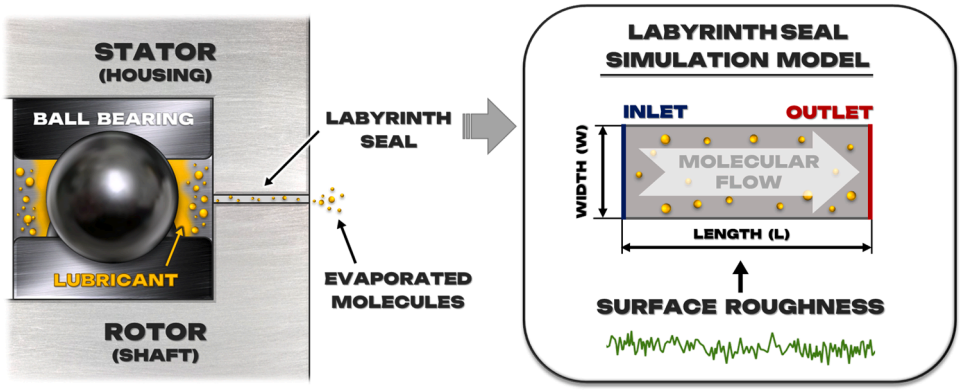

Fig. 1. Visualization of a ball bearing system with an integrated labyrinth seal and evaporating molecules, coupled with a simulation model incorporating surface roughness geometry.

The spectral envelope *h(n)* attenuates high-frequency components. The spectral exponent *b* controls the rate of amplitude decay with frequency, while *g(n)* is a Gaussian random function with zero mean and unit variance. Since the resulting function *f(x)* is inherently periodic, only a subdomain (i.e., [0, 1]) was extracted to mitigate visible periodicity in the final geometry.

In practice, roughness profiles were implemented in COMSOL as parametric curves, representing height perturbations. These curves were then extruded to form the sidewalls of the labyrinth seal corridor. Each curve was generated using a spectral synthesis function combining Gaussian (*g*) and Uniform (*u*) random distributions, expressed as

$$z = PC \bullet \sum_{n=-N}^{N} \left(n^2\right)^{-\frac{b}{2}} \cdot g(n) \bullet \cos(2\pi(nx) + u(n)) \tag{5}$$

Here, *N* is the spatial frequency resolution, and *b* is the spectral exponent controlling amplitude decay with frequency. The scaling factor, referred to as the parametric curve (*PC*) coefficient, was varied to generate different roughness amplitudes. Multiple values of *PC* were applied across simulations for each (*N, b*) pair to produce a comprehensive range of surface roughness levels. These curves were interpolated and applied to the geometry boundaries in COMSOL, enabling precise control of wall roughness during meshing and simulation.

2.2. Surface generation and evaluation of surface roughness profiles

To investigate how mathematical parameters influence the physical characteristics of surface topography, a parametric study was conducted by systematically varying the *N, b* and *PC*. These parameters define the surface structure in the spatial frequency domain:

- *N* controls the spatial resolution, determining the number and density of peaks,
- *b* governs the rate of amplitude attenuation across frequencies,
- *PC* scales the overall amplitude of the roughness profile.

A comprehensive set of synthetic surface profiles was generated for a range of *N, b* and *PC* combinations (see Fig. 2) summarized in Table 1. This results in a comprehensive grid of synthetic surfaces designed to probe both low-frequency (coarse) and high-frequency (fine) features under different amplitude scaling regimes. Several widely used surface roughness parameters were extracted from each profile, as one parameter cannot adequately describe the surface properties [34]. These parameters are further described together with their mathematical definitions, and responses to the varying spectral inputs. The resulting data provided a foundation for selecting representative surfaces used in subsequent molecular flow simulations.

2.2.1. Arithmetic mean roughness (Ra)

The arithmetic mean roughness is one of the most used surface roughness parameters in engineering [15,35]. It represents the average of the absolute deviations from the mean line of the surface profile and

Table 1
Overview of adjustable parameters used to simulate surface topography.

Parameter	Range	Step
N	10 – 100	10
b	0.05 – 0.5	0.05
PC	0.001 – 0.003	0.001

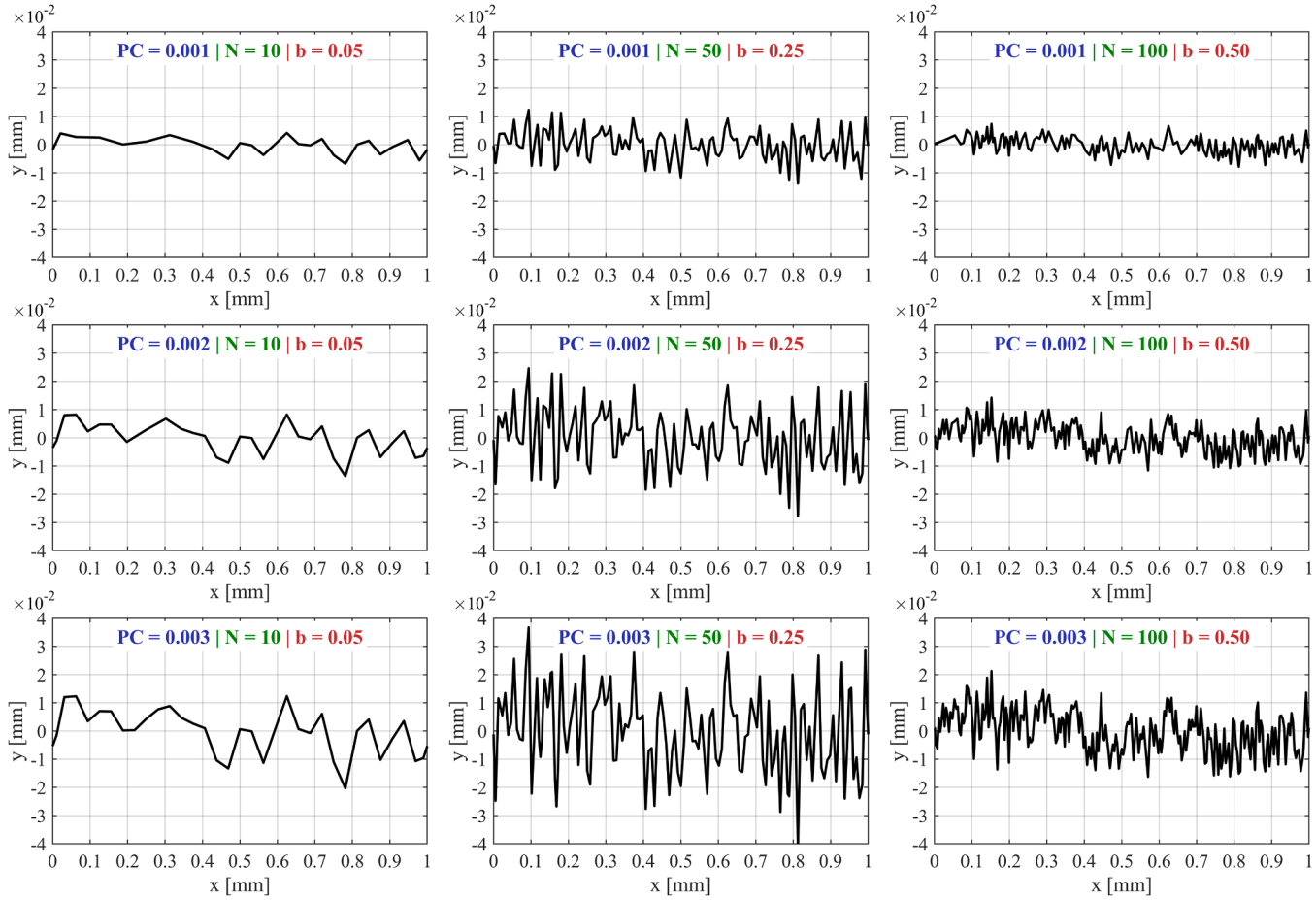

Fig. 2. Synthetic surface roughness profiles generated for varying spectral resolution (*N*), spectral exponent (*b*) and parametric curve coefficients (*PC*).

gives a general indication of surface height variation [36–38].

$$Ra = \frac{1}{L}\int_0^L |z(x)|\, dx \;\approx\; \frac{1}{m}\sum_{i=1}^{m} |z_i| \tag{6}$$

where z_i are the discrete height values of the profile and m is the number of data points. The Fig. 3(i) shows the variation of the *Ra* as a function of *N* and *b* for different values of the *PC*. As expected, increasing *N* introduces finer spatial details, while decreasing *b* results in rougher, more irregular surfaces with higher *Ra* values. Across all simulations, *Ra* increases nearly linearly with *PC*, confirming its primary role in scaling the vertical amplitude of the roughness profiles. Surfaces generated with lower *N* and higher *b* generally exhibit lower *Ra* values. However, as *PC* increases, its influence becomes more dominant, leading to a pronounced amplification of surface roughness regardless of the underlying spectral characteristics.

2.2.2. Root mean square roughness (Rq)

The root mean square roughness quantifies the standard deviation of the surface height. Calculated values are similar to *Ra* but emphasizes larger deviations due to squaring the profile values [36–38].

$$Rq = \sqrt{\frac{1}{L}\int_0^L z^2(x)\, dx} \;\approx\; \sqrt{\frac{1}{m}\sum_{i=1}^{m} z_i^2} \tag{7}$$

The root mean square roughness is particularly valuable in applications where sensitivity to outlier features or overall roughness energy is critical. Compared to *Ra, Rq* typically yields slightly higher values for the same surface due to its squared deviation weighting. Fig. 3(ii) shows the influence of the spectral parameters *N* and *b* on *Rq* for various *PC* values. The observed trends closely mirror those of *Ra*, with *Rq* generally increasing as *N* increases and *b* decreases, reflecting the heightened surface complexity. As expected, *Rq* values consistently exceed *Ra* due to the squaring of height deviations in its calculation.

2.2.3. Skewness (Rsk)

Skewness quantifies the asymmetry of a surface profile about its mean line. A negative *Rsk* indicates a prevalence of valleys, while a positive *Rsk* suggests a prevalence of peaks [38].

$$Rsk = \frac{1}{Rq^3} \bullet \frac{1}{L}\int_0^L z^3(x)dx \;\approx\; \frac{1}{Rq^3} \bullet \frac{1}{m}\sum_{i=1}^{m} (z_i - \bar{z})^3 \tag{8}$$

Skewness (see Fig. 3 (iii)) is primarily influenced by the spectral resolution N: low *N* tends to produce surfaces with deep valleys and sharp peaks, resulting in more pronounced asymmetry. In contrast, high *N* yields smoother, more balanced surfaces, causing skewness to approach zero regardless of the *PC* value. The effect of the spectral exponent *b* on skewness is relatively minor compared to *N* and PC. Surfaces generated with the lowest *PC* (i.e., 0.001) exhibit the most irregular and unpredictable skewness values. As *PC* increases, these irregularities are reduced, and skewness becomes more stable across different spectral configurations.

2.2.4. Kurtosis (Rku)

Kurtosis characterizes the profile's deviation from a Gaussian distribution in terms of the concentration of surface features [38]. A value of $Rku = 3$ corresponds to a normal (Gaussian) distribution. Values greater than 3 (leptokurtic) suggest the presence of pronounced peaks or deep valleys, while values <3 (platykurtic) indicate a flatter surface topology.

$$Rku = \frac{1}{Rq^4} \bullet \frac{1}{L}\int_0^L z^4(x)dx = \frac{1}{Rq^4} \bullet \frac{1}{m}\sum_{i=1}^{m} (z_i - \bar{z})^4 \tag{9}$$

The results in Fig. 3(iv) suggests that kurtosis does not consistently increase with spectral resolution (N). Instead, the spectral exponent (*b*), which controls the damping of high-frequency components, appears to have a greater influence: as *b* decreases, isolated protrusions and depressions become more pronounced, theoretically leading to higher kurtosis values. Additionally, kurtosis decreases with increasing *PC*, gradually approaching the Gaussian reference value of 3. This trend indicates that surfaces with low *PC* retain sharper features and more isolated peaks or valleys, while higher *PC* values smooth these extremes by scaling the amplitude, resulting in profiles with fewer distinct high or low points.

2.2.5. Bearing curve parameters (Rk, Rpk, Rvk)

The bearing (Abbott-Firestone) curve parameters provide insight into the functional performance of a surface [38–41]. These include the core roughness depth (*Rk*), reduced peak height (*Rpk*) above the core material, and reduced valley depth (*Rvk*), which are extracted by fitting the linear portion of the material ratio curve and extrapolating to estimate the peak and valley contributions [14,19,37,18].

These roughness parameters are closely influenced by machining processes, especially turning, where characteristics such as *Rk, Ra* and *Rq* often display a near-linear relationship with the feed rate [37,40,18]. This correlation enables reliable prediction and modelling of surface topography based on known cutting speeds and feed conditions [42,43].

Bearing curve parameters *Rk, Rpk*, and *Rvk* (see Fig. 4) follow trends similar to those observed for *Ra* and *Rq*, exhibiting consistent dependence on the spectral parameters *N, b*, and *PC*. The core roughness depth (*Rk*) generally decreases with increasing *b*, indicating smoother surfaces as high-frequency components reduce the vertical extent of the load-bearing region. All three parameters scale approximately linearly with *PC*, reaffirming its role as a vertical amplification factor. These findings highlight the sensitivity of functional surface parameters to both spectral shape and amplitude scaling. Their combined evaluation offers deeper insight into the evolution of surface topography and its potential impact on contact mechanics and tribological performance.

2.3. Molecular flow simulation setup

To evaluate the influence of surface roughness on molecular flow behaviour, a series of simulations were conducted using COMSOL Multiphysics 6.3, under free molecular flow conditions. The geometry of the model consisted of a 2D labyrinth seal corridor defined by inlet and outlet boundaries and two parallel walls formed by the synthetic surface roughness profiles.

To ensure geometric symmetry and isolate the effect of surface topography, the same parametric curve was used for both labyrinth walls. Specifically, the roughness profile was first generated for one wall (lower boundary), and the second wall (upper boundary) was created by duplicating this curve and shifting it vertically along the y-axis by a distance equal to the labyrinth width. This setup ensured that both walls had matching roughness features, avoiding discrepancies caused by independent wall geometries.

The simulations were run under isothermal high-vacuum conditions, with molecular properties based on Fomblin Y LVAC 25/6 a perfluoropolyether (PFPE) lubricant used in prior experimental validation studies [3,5]. The geometrical dimensions, meshing settings, simulation parameters, and fluid properties used in the simulations are summarized in Table 2.

Geometrical parameters including channel length and width were varied systematically to assess how confinement and seal dimensions interact with surface roughness. The analysis of the simulation results focused on two key evaluation metrics: the transmission probability and the molecular flux at the outlet. The transmission probability (*TP*) provides a dimensionless measure of flow efficiency [5,44,45]

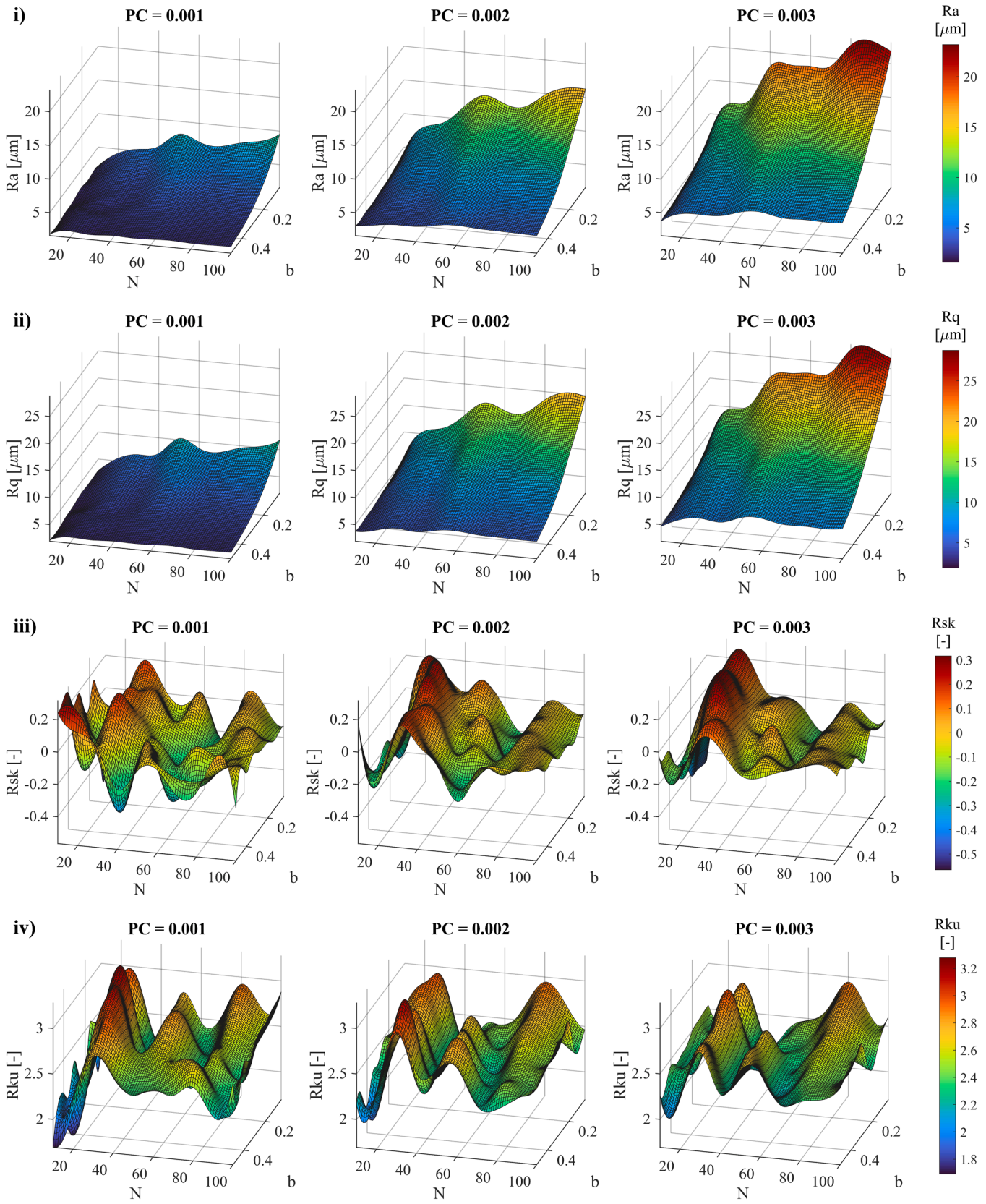

Fig. 3. Surface roughness parameters vs spectral parameters *N* and *b* for varying *PC*: Ra (i), Rq (ii), Rsk (iii), Rku (iv).

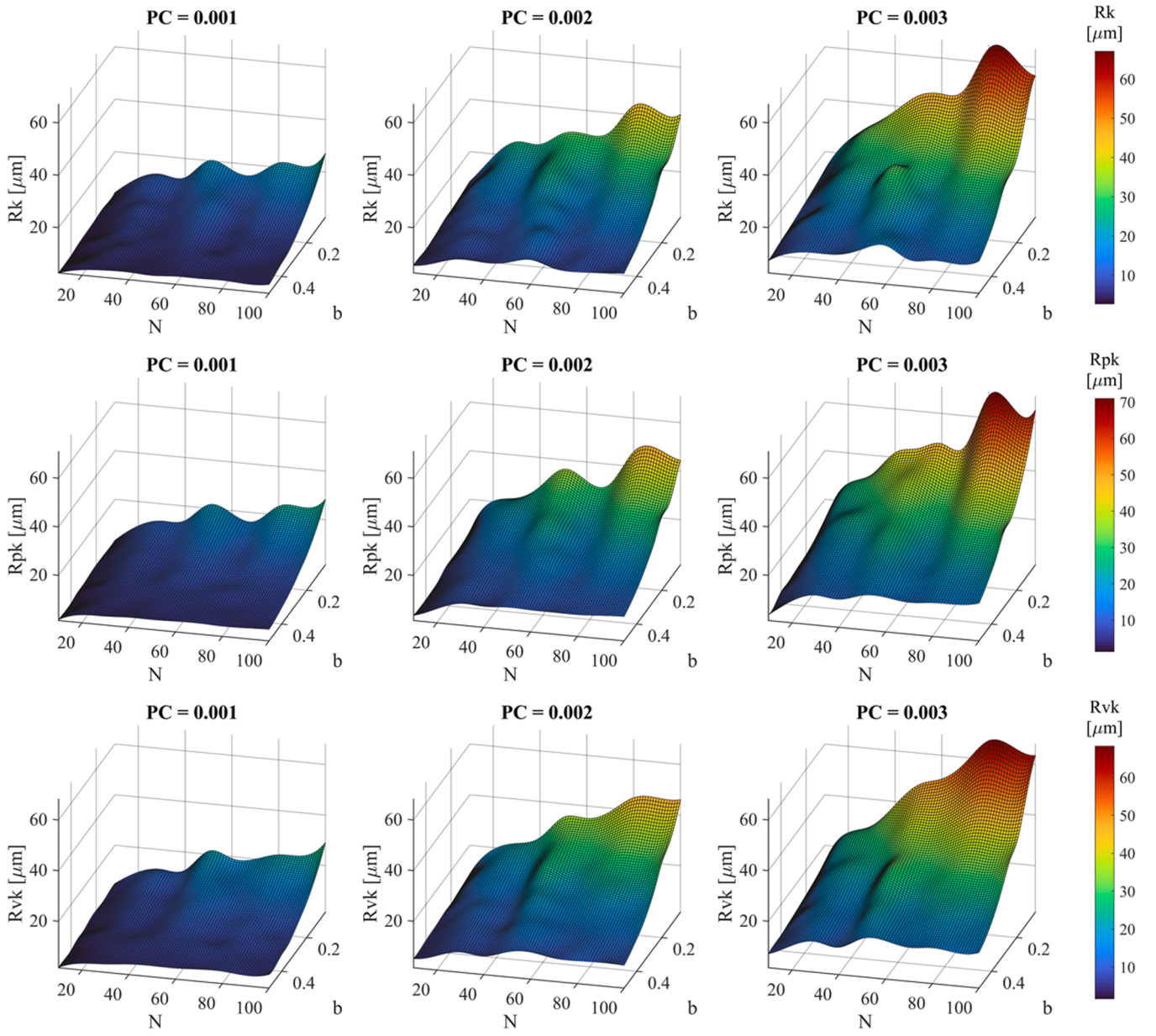

Fig. 4. Bearing curve parameters *Rk, Rpk*, and *Rvk* across *N, b*, and *PC*.

Table 2
Summary of simulation parameters and lubricant properties used for molecular flow simulations.

Category	Parameter	Value	Description
Geometry	Labyrinth length (L)	1 – 10 mm	Parametrically varied to evaluate length influence
	Labyrinth width (W)	0.2 – 1.0 mm	Parametrically varied to study confinement effects
Meshing	Grid resolution	Physics-controlled	Refined mesh near boundaries for surface details
Simulation conditions	Temperature (T)	373.15 K	Isothermal condition across the domain
	Inlet pressure	6E-4 Pa	Define as per boundary condition
	Outlet pressure	Total vacuum	Typically vacuum or near-zero pressure
Oil sample	Lubricant name	Fomblin Y LVAC 25/6	Perfluoropolyether (PFPE) lubricant
	Molecular weight	~3300 g/mol	Molecular mass used for molecular flow simulations

$$TP = \frac{\boldsymbol{N}_1}{\boldsymbol{N}_0} \tag{10}$$

where N_0 represents the total number of molecules entering the channel, and N_1 corresponds to the number of molecules successfully exiting through the outlet. This metric offers a clear and intuitive indication of the sealing performance of the labyrinth geometry and is particularly valuable in molecular flow regimes [5,44]. Its normalized form allows for greater generalization of results across varying boundary conditions, which is critical for the development of simulation-based correction functions introduced in later sections of this work.

In contrast, the mass flow at the outlet, which represents the absolute number of molecules per unit area and time reaching the exit, is more directly tied to the specific pressure and temperature conditions imposed in the simulation. While it provides additional physical insight and supports validation with experimental measurements, it is less transferable across scenarios without recalibration. Therefore, transmission probability was prioritized as the central comparative metric in this study, serving as the foundation for assessing how variations in

surface roughness affect molecular flow through the seal.

To systematically assess the influence of each parameter on transmission behaviour, three representative datasets were selected for detailed simulation (see Table 3), covering a wide spectrum of roughness structures from coarse, low-frequency features to finely resolved microstructures. The selected datasets span a broad range of spectral configurations, from coarse, low-frequency structures to finely resolved, high-frequency surfaces.

Among the evaluated parameters, the *PC* factor plays a primary role in scaling the amplitude of surface profiles and thus has a direct influence on amplitude-related roughness metrics such as *Ra, Rq, Rk, Rpk*, and *Rvk*. These parameters exhibited nearly linear increases with *PC*. The skewness (*Rsk*) and kurtosis (*Rku*) demonstrated more nuanced, nonlinear responses, particularly at lower *PC* values. These findings highlight the complex interplay between spectral structure and vertical scaling in determining the overall surface character. The datasets cover a range of surface morphologies, from dominant low-frequency fluctuations to compactly arranged fine features.

3. Results

To evaluate the influence of surface roughness on molecular transport, synthetic roughness profiles were generated through a parametric sweep of three key variables: spectral resolution (N), spectral exponent (b), and vertical scaling factor (PC). These parameters respectively govern the spatial frequency content, spectral decay, and amplitude of the surface profiles. The transmission probability results, evaluated across the three amplitude scaling values are summarized in Fig. 5.

The results show that increasing N significantly reduces transmission probability (*TP*), following a second-order trend. In contrast, decreasing *b* leads to an approximately linear drop in *TP*, indicating that low-frequency roughness features play a key role in impeding molecular passage. Variations in *PC* influence the curvature of the *N–TP* relationship. Higher PC values cause transmission probability to decline more steeply at low N, amplifying the impact of roughness height on molecular transmission.

A 2D contour analysis of *TP* and *Ra* across *N* and *b* for different *PC* values (see Fig. 5) confirms a consistent inverse relationship where *TP* decreases consistently with increasing *Ra*. This underscores how spectral parameters shape surface morphology and influence molecular flow.

3.1. Characterization of synthetic surface roughness datasets

The synthetic roughness datasets (see Table 3) were integrated into COMSOL Multiphysics simulations of molecular flow through 2D labyrinth seal geometries. For each surface profile, the labyrinth corridor was constructed with matching wall curves, and simulations were run across multiple channel widths and lengths as summarized in Table 2. This approach enabled an in-depth examination of how surface roughness, when interacting with geometry, influences transmission probability and molecular flux.

For each dataset, surface profiles were generated and evaluated using standard roughness metrics, including amplitude parameters (*Ra, Rq, Rk, Rpk, Rvk*) and shape descriptors (*Rsk, Rku*). The trends observed across the *PC* sweep reveal how different spectral configurations influence the geometry and statistical properties of the rough surfaces.

Table 3
Overview of parameter sets used for surface generation in molecular flow simulations.

Dataset	Spectral resolution N	Spectral exponent B	Roughness amplitude scaling	
			PC	Number of steps
1	30	0.5	0.0005 to 0.020	12
2	50	0.05	0.0001 to 0.002	11
3	100	0.1	0.0001 to 0.001	10

3.1.1. Dataset 1 – moderate resolution, coarse structures

Dataset 1 represents rough surfaces dominated by low-frequency fluctuations with clearly defined peaks and valleys. The spectral resolution is moderate ($N = 30$) and the relatively high spectral exponent ($b = 0.5$) emphasizes large-scale features. This dataset is particularly suited to evaluate how prominent topographical features scatter molecular trajectories.

The amplitude-related surface roughness parameters (*Ra, Rq, Rk, Rpk, Rvk*) increased approximately linearly with *PC* (see Fig. 6). In contrast, the shape descriptors *Rsk* and *Rku* demonstrated nonlinear behaviour, especially at low *PC* values, indicating enhanced asymmetry and peak sharpness at small amplitudes.

3.1.2. Dataset 2 – high resolution, broad variability

In Dataset 2, the spectral resolution is increased to $N = 50$ and the spectral exponent is reduced to $b = 0.05$. This configuration results in surface profiles with weaker spectral decay and more uniformly distributed spatial frequencies resembling a white noise texture. The result is a high-frequency surface rich in fine structure and randomness.

Despite the increase in resolution, the amplitude parameters continue to scale predictably with *PC* (see Fig. 7). However, *Rsk* and *Rku* show greater sensitivity and fluctuation due to the fine-scale randomness becoming more pronounced at higher spatial resolution.

3.1.3. Dataset 3 – very high resolution, fine-scale features

Dataset 3 explores the limits of spectral resolution with $N = 100$ and a moderate spectral exponent ($b = 0.1$), generating highly detailed profiles with dense, fine-scale features. To isolate the influence of small amplitude variations, *PC* values are constrained to a narrow range ($0.0001 – 0.001$).

The increased resolution led to a denser distribution of surface irregularities, which strongly affects molecular scattering even at minimal vertical scaling. The effect of *PC* on all roughness parameters was less pronounced in absolute terms (see Fig. 8).

3.2. Combined analysis across datasets

The synthetic surface roughness profiles described in Section 3.1 were incorporated into COMSOL Multiphysics simulations to assess their influence on molecular transport through 2D labyrinth seal geometries. For each profile, a matching channel geometry was constructed by embedding the corresponding surface curve into both walls of the labyrinth (see Fig. 1). Simulations were performed for a range of corridor widths ($W = 0.2 – 1$ mm) and lengths ($L = 1 – 10$ mm), as summarized in Table 2.

Each rough surface configuration was benchmarked against a smooth-wall reference ($Ra = 0$), enabling quantitative evaluation of how surface roughness impedes molecular flow. Across all datasets, an increase in surface roughness (i.e., higher *PC* values) consistently resulted in lower transmission probabilities (see Fig. 9). The smooth reference surface exhibited the highest transmission probability across all geometries.

The effects of roughness were modulated by both corridor length and width (see Fig. 10):

- Corridor Length (*L*): Longer channels provided more opportunities for molecule-wall interactions. This resulted in cumulative scattering effects, especially for profiles with high spectral resolution. For these cases, the transmission probability often exhibited exponential decay with length.

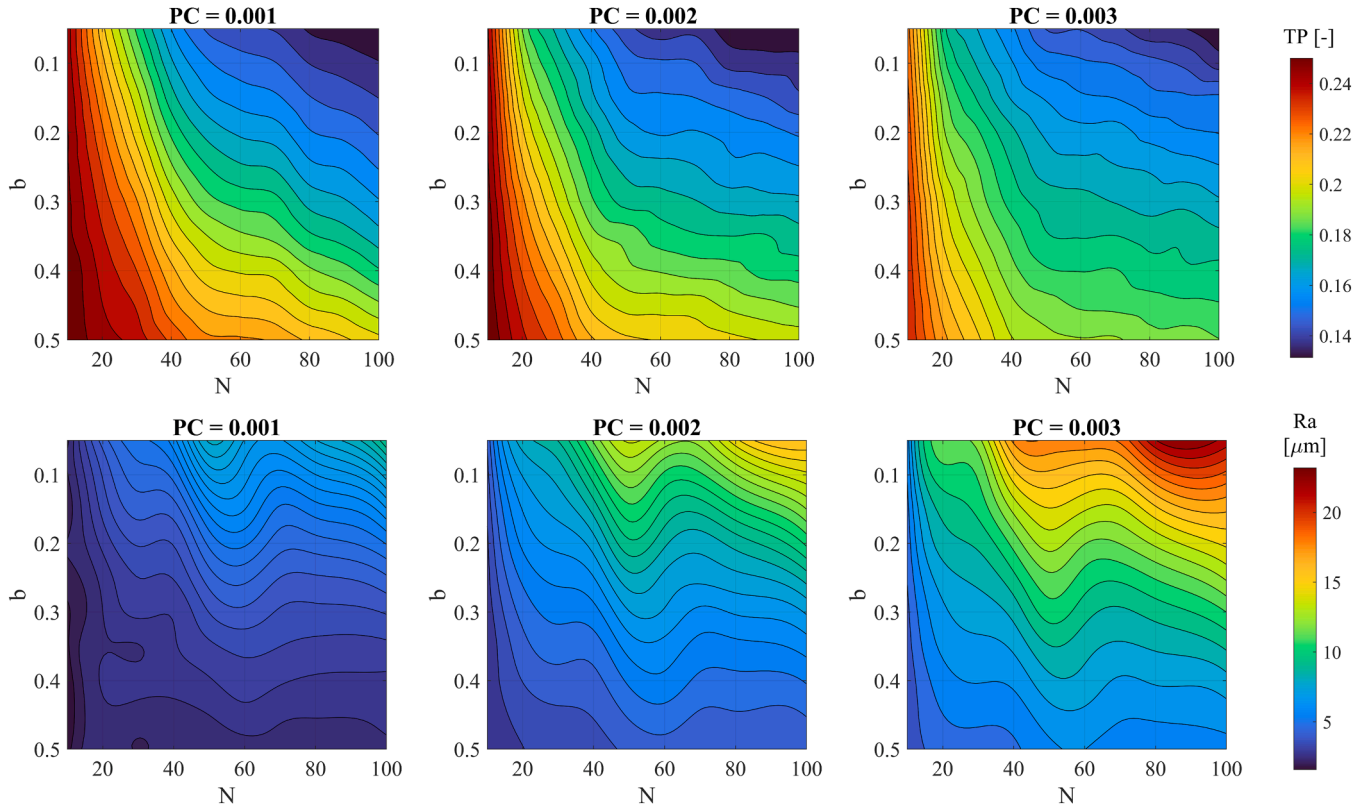

Fig. 5. Contour plots of transmission probability (*TP*) and average roughness (*Ra*) as functions of spectral parameters *N* and *b* for varying amplitude scaling (*PC*).

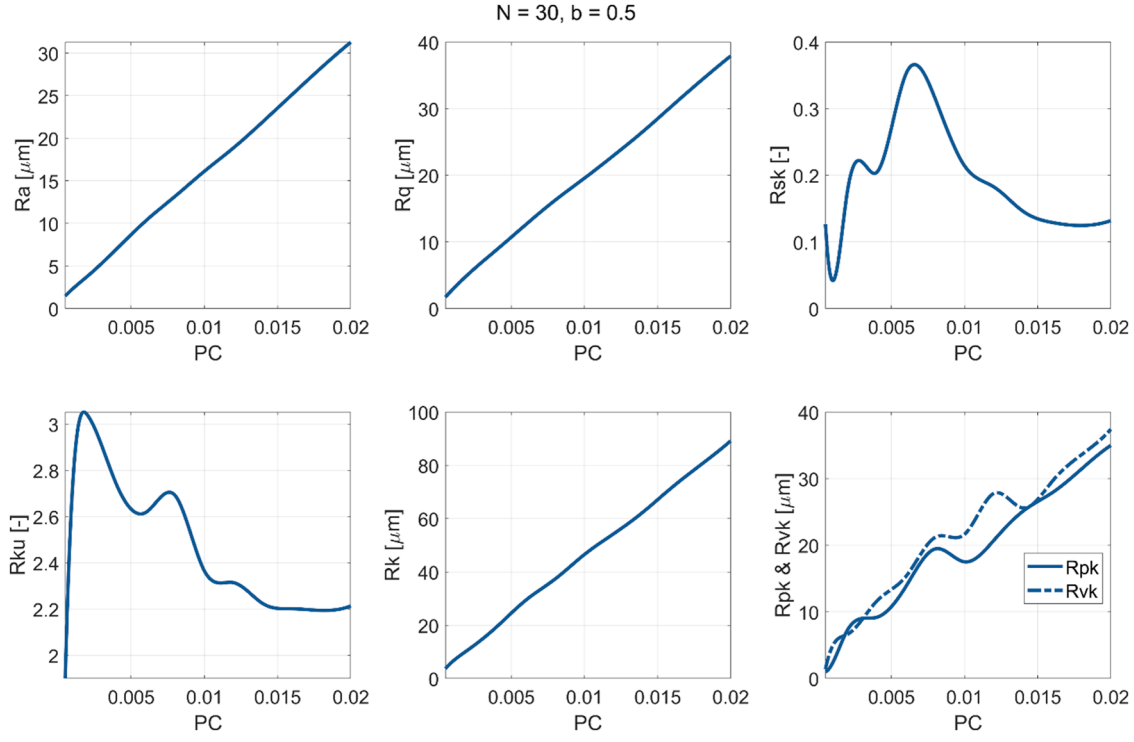

Fig. 6. Surface roughness parameters as a function of *PC* (Dataset 1, $N = 30$, $b = 0.5$).

- Corridor Width (*W*): In narrow geometries, molecular trajectories are more frequently intercepted by rough walls, amplifying the effect of surface irregularities. This led to steep, often nonlinear declines in transmission probability even at moderate *Ra* values. Wider channels demonstrated a reduced sensitivity, though the damping effect of roughness remained evident.

To systematically describe these dependencies, second-order

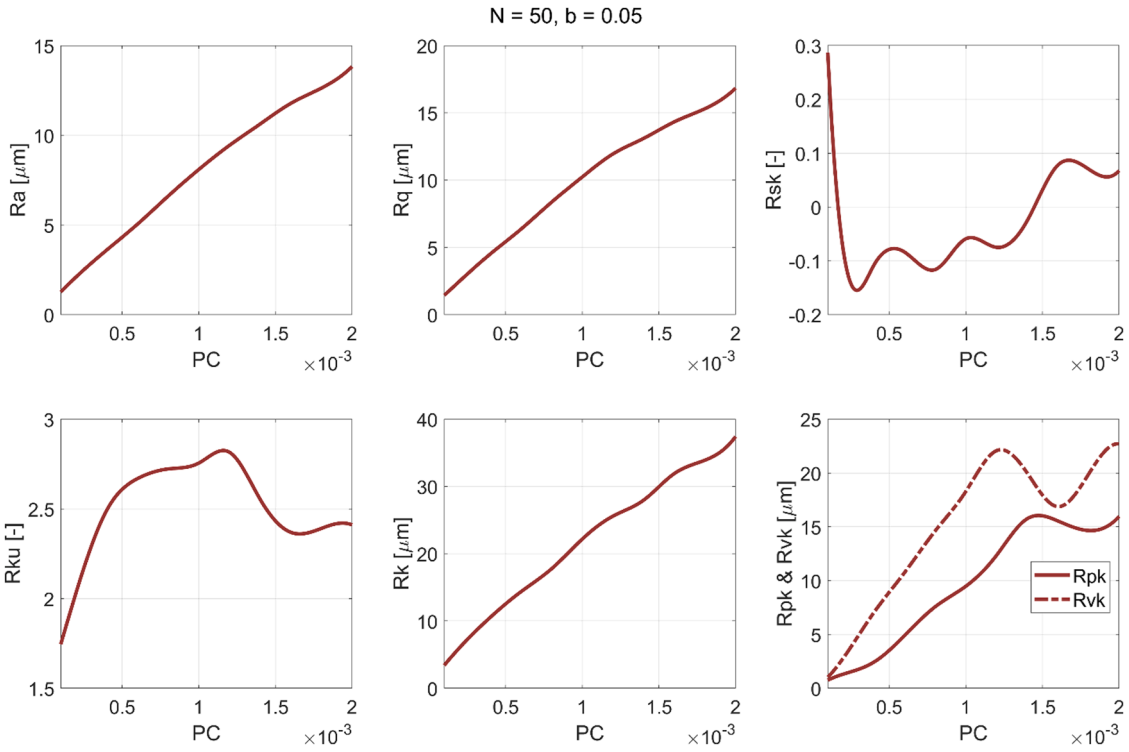

Fig. 7. Surface roughness parameters as a function of *PC* (Dataset 2, $N = 50$, $b = 0.05$).

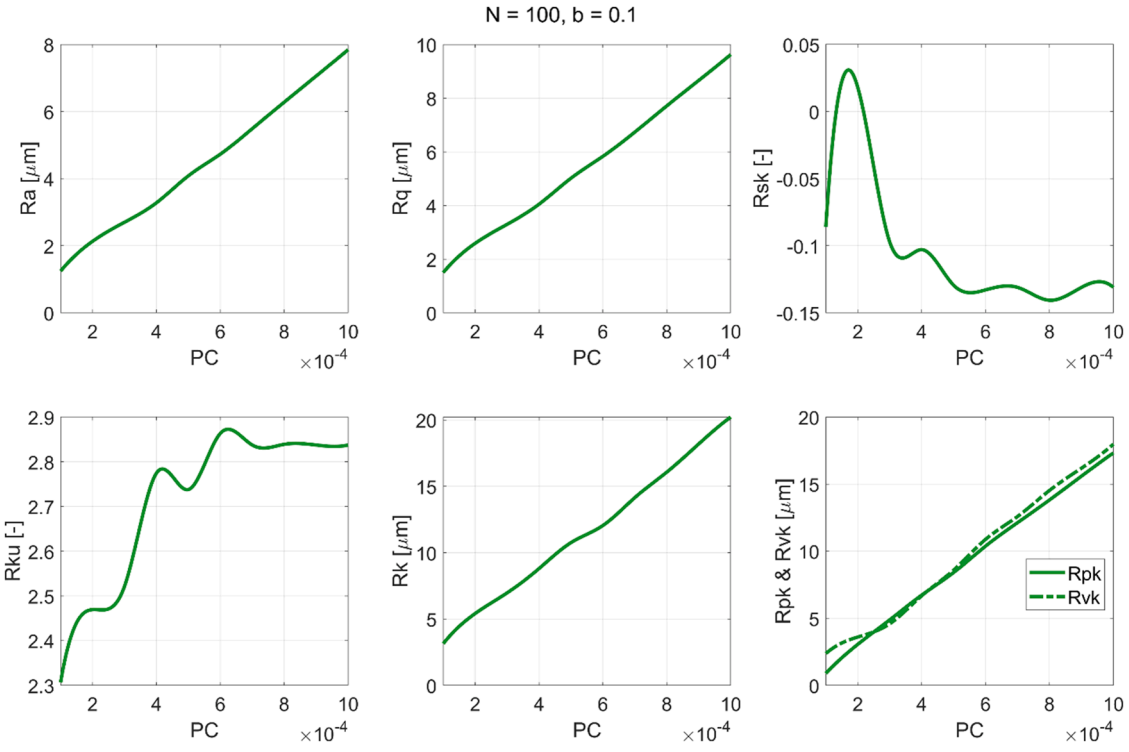

Fig. 8. Surface roughness parameters as a function of *PC* (Dataset 3, $N = 100$, $b = 0.1$).

polynomial fits of transmission probability versus *Ra* were computed for each (*W, L*) combination. The coefficients of these fits revealed clear trends, highlighting how both the amplitude and spectral characteristics of surface roughness affect flow resistance. These trends offer a foundation for developing correction models or relationships to estimate *TP* in rough microchannels.

3.3. Simulation-based correction model

Based on the extensive simulation results presented in Sections 3.1 and 3.2, a clear relationship was established between transmission probability (*TP*), surface roughness characteristics, and labyrinth geometry. These insights formed the basis for developing a simulation-

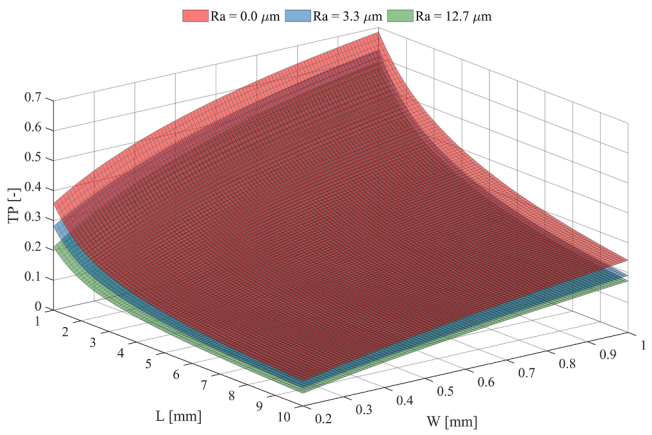

Fig. 9. Transmission probability across labyrinth length and width for varying surface roughness.

based correction model that estimates *TP* in 2D labyrinth seals as a function of surface roughness (quantified by *Ra*), and corridor geometry (length *L* and width *W*).

3.3.1. Model structure

From the simulation data, transmission probability was found to follow a smooth, nonlinear trend when plotted against *Ra* for fixed *W* and *L*. This trend was best captured by following second-order polynomial fit for calculating the corrected transmission probability (*TP*):

$$TP\ (\boldsymbol{Ra},\ \boldsymbol{W},\ \boldsymbol{L}) = A(\boldsymbol{W},\boldsymbol{L}) \bullet \boldsymbol{Ra}^2 + B(\boldsymbol{W},\boldsymbol{L}) \cdot Ra + C(W,L) \tag{11}$$

where *A(W, L), B(W, L), C(W, L)* are polynomial coefficients dependent on the geometric configuration and *Ra* is the arithmetic mean roughness (in μm). The coefficients were extracted from the simulation results by fitting curves to *TP* vs. *Ra* for each unique (*W, L*) combination. This generated a 3D matrix of coefficients [$A_{i,j}$, $B_{i,j}$, $C_{i,j}$] indexed by width and length, enabling interpolation or surface fitting across arbitrary geometries within the studied range. The complete set of fitted coefficients for all simulated W and L combinations is provided in the supporting data (see Data Availability Statement), allowing it to directly apply the correction model.

3.3.2. Model application

The developed correction model estimates the transmission probability (TP) of molecules through a labyrinth seal based on the surface roughness parameters of the seal walls, eliminating the need for extensive simulations. To apply the model:

1. Determine the surface roughness *Ra* (e.g., from measurement or simulation).
2. Identify the target channel dimensions (*W, L*).
3. Obtain the corresponding polynomial coefficients *A(W, L), B(W, L)* and *C(W, L)* from the supporting dataset provided with this study (see Data Availability Statement).
4. Calculate the transmission probability using the correction function Eq. (11).

This approach enables fast and flexible prediction of *TP* for design evaluations, roughness tolerance analyses, or process sensitivity studies. The model is especially valuable in the early stages of seal design, where quick estimations are critical for parameter screening and trade-off assessments. The correction function is valid within the range of parameters studied in the simulations:

- Surface roughness (*Ra*) up to approximately 13 μm
- Channel widths (*W*) of 0.2 – 1 mm
- Channel lengths (*L*) of 1 – 10 mm

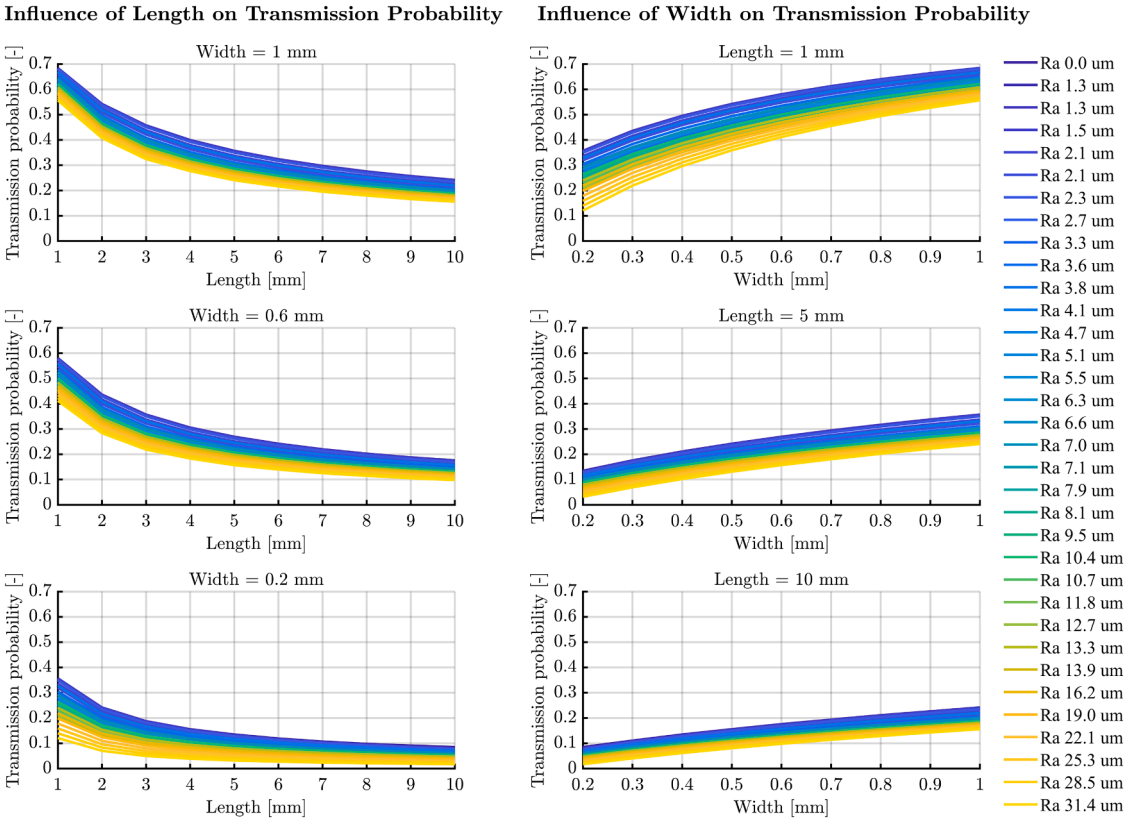

Fig. 10. Length and width effects on transmission probability across all surface roughness datasets.

Limitations should be noted when applying the model outside this parameter space. At extreme values (very high roughness or ultra-narrow channels) extrapolated predictions may diverge from actual physical behaviour due to geometric confinement or surface interactions not fully captured in the polynomial fit. Moreover, while the model captures the influence of roughness amplitude, it does not explicitly account for spectral characteristics (e.g., slope, spatial frequency), which may further influence molecular scattering. Future improvements could incorporate such features, for instance by introducing a spectral weighting term based on the roughness exponent b, or by including secondary metrics like the Rq/Ra ratio.

In summary, the model serves as a reliable and efficient tool for estimating molecular flow performance in rough microchannels, with potential for further extension to account for additional roughness descriptors and more complex geometries.

3.3.3. Model validation with experimental data

To evaluate the predictive capability of the proposed correction model, a comparison was made against experimentally measured evaporative mass losses through two labyrinth seal configurations exhibiting different surface roughness levels. These experiments, conducted in prior work [5], assessed the sealing performance of various labyrinth configurations during vacuum evaporation of a liquid lubricant.

All labyrinth seals shared identical channel dimensions: length $L = 10$ mm and width $W = 0.5$ mm, ensuring that the only varying factor was the surface roughness (see Table 4). For validation, an Ideal labyrinth with zero surface roughness ($Ra = 0$ μm) was introduced as a baseline reference to which the transmission probability (TP) predictions from the correction model were normalized (see Table 5). The experimental configurations (Labyrinth 1 and Labyrinth 2) were characterized using a Bruker Contour GTX 3D optical profilometer.

The model-predicted transmission probabilities (TP) for all three seals were calculated using the correction function Eq. (11). These values were then normalized relative to the Ideal labyrinth ($Ra = 0$ μm) to highlight the effect of roughness on molecular transport. To validate the model's predictive accuracy, the predicted TP ratios were then compared against the experimental ratios of evaporative mass loss, which serve as a physical proxy for relative transmission probability. This comparison approach provides insight into both the model's theoretical consistency and its empirical relevance. The results are summarized in Table 5.

These results confirm that the proposed correction model provides reliable prediction of molecular transport through rough labyrinth geometries, with a relative error of 5.1 % in the tested range. The close agreement demonstrates the robustness of the Ra-driven model structure and supports its practical applicability in early design and tolerance studies of microstructured channels under molecular flow.

Nonetheless, it should be noted that the correction model remains simulation-based and may deviate when applied beyond the calibration range (e.g., ultra-high Ra, channel widths below 0.2 mm, or non-uniform 3D roughness distributions). Additional experimental validation, including more diverse surface profiles and spectral characterizations, would further improve confidence in the model and enable potential extensions.

Table 4
Ideal and experimental conditions for labyrinth seal validation.

Category	Parameter	Value
Ideal labyrinth	Length (L)	10 mm
	Width (W)	0.5 mm
	Evaporative mass loss	–
	Surface roughness	Ra 0.00
Labyrinth 1	Length (L)	10 mm
	Width (W)	0.5 mm
	Evaporative mass loss	3.8 mg/h
	Surface roughness	Ra 0.13
Labyrinth 2	Length (L)	10 mm
	Width (W)	0.5 mm
	Evaporative mass loss	3.3 mg/h
	Surface roughness	Ra 3.88

Table 5
Comparison of model-predicted and experimentally measured transmission probability (TP) ratios for two labyrinth seals with different surface roughness levels.

	Ideal Labyrinth	Labyrinth 1	Labyrinth 2
Model-predicted TP	0.2933	0.2924	0.2670
TP ratio (vs. Ideal Labyrinth)	1.0000	0.9968	0.9104
Measured evaporative loss	–	3.8 mg/h	3.3 mg/h
Evaporative loss ratio (vs. Labyrinth 1)	–	1.0000	0.8684
Predicted TP ratio (vs. Labyrinth 1)	–	1.0000	0.9131
Relative error (prediction vs. measurement)	–	0.0 %	5.1 %

4. Discussion

The simulation results demonstrated a consistent inverse relationship between surface roughness and transmission probability (TP). As the average roughness Ra increased, TP decreased across all straight labyrinth configurations. This trend was especially pronounced in narrower and longer channels, where increased confinement and extended interaction paths led to a higher likelihood of molecule-wall collisions. These findings highlight that even moderate increases in surface irregularity can result in measurable reductions in molecular flow.

All simulations were run under isothermal conditions with a constant wall temperature without considering the thermal expansion of material. Chemical interactions and surface reactions were excluded, and material-dependent accommodation was not modeled. These assumptions isolate the effect of geometric roughness on transmission probability.

The data exhibit a clear decreasing trend of TP as surface roughness increases. A quadratic curve was fitted to the data to visualize the general trend (see Fig. 11) for one set of labyrinth seal dimensions ($W = 0.5$ mm, $L = 10$ mm). The parabolic shape of the fitted curve confirms that even moderate increases in roughness lead to non-linear reductions in TP. Interestingly, the curve begins to flatten at higher roughness

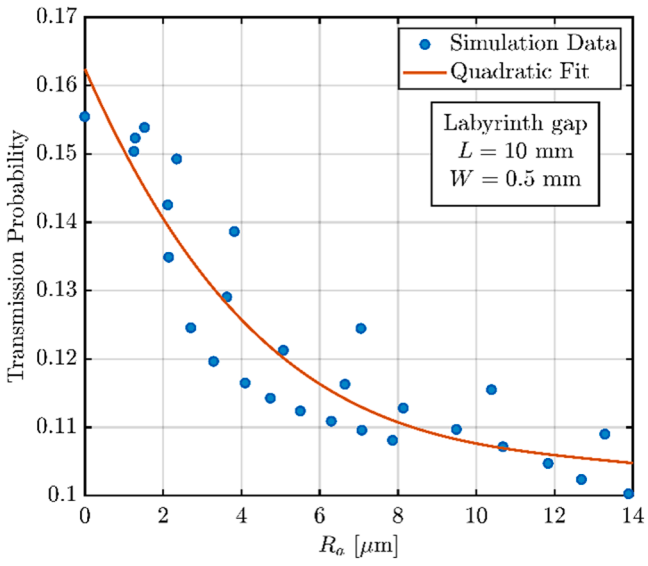

Fig. 11. Transmission probability vs. surface roughness ($W = 0.5$ mm, $L = 10$ mm).

levels, suggesting a saturation regime where further increases in roughness cause diminishing effects on *TP*.

Labyrinth seal corridor width (*W*) and length (*L*) were shown to modulate the effect of surface roughness non-linearly. Narrower channels amplified the influence of surface asperities by increasing the probability of collisions per unit path length, while longer channels introduced a cumulative scattering effect. This aligns with theoretical expectations in the molecular flow regime [5,26,46], where the mean free path exceeds the characteristic geometry, and the interactions of molecules with the wall dominate the transport behaviour. The strength of this geometric dependence justified the development of a simulation-based correction model.

This second-order polynomial correction model successfully generalized transmission probability across all datasets. Despite the variation in spectral properties (e.g., different *N* and *b* values), the dominant influence on *TP* was clearly attributed to the amplitude of surface roughness (*Ra*), rather than its spectral distribution. This allowed the model to be simplified without compromising predictive power for most practical configurations.

The model's predictive performance was validated by comparison with two experimental measurements of evaporative mass loss in previously tested labyrinth seals [5]. The correction model predicted *TP* ratios with a relative error of 5.1 %, demonstrating high agreement with physical observations. This confirms the model's utility for estimating molecular flow losses in seals with known surface roughness characteristics.

In addition to its predictive capabilities, the simulation data revealed a valuable design implication: surface roughness can serve as a compensatory parameter for geometric constraints in labyrinth seal design. Specifically, increasing the average roughness amplitude (*Ra*) allows for either a reduction in channel length or an increase in gap width of approximately 35–40 %, while maintaining a constant transmission probability (see Fig. 12). This finding underscores the potential of controlled surface texturing as a strategic approach to reduce molecular flow losses, enhance design flexibility, and improve the compactness and manufacturability of vacuum labyrinth seal systems.

Despite the model's strengths, several limitations must be acknowledged. The use of synthetically generated surface profiles may not fully capture the statistical complexity, anisotropy, or localized defects present in real-world machined or worn surfaces [17,37], potentially limiting the model's applicability to actual engineering conditions. Additionally, the simulations are restricted to a two-dimensional (2D) domain, which simplifies the inherently three-dimensional (3D) nature of practical labyrinth geometries. Effects such as edge curvature, cross-sectional variation, and out-of-plane confinement may alter molecular flow in ways not represented here.

The model also relies on the average roughness parameter (*Ra*) as a scalar descriptor of surface morphology. While effective for capturing broad trends in transmission probability, *Ra* omits higher-order surface characteristics such as skewness, kurtosis, or peak-valley asymmetry, which could influence flow behavior, particularly in more irregular or asymmetric profiles. Furthermore, the model does not account for temperature effects [1,4,47] or material specific gas-surface interactions, such as adsorption, desorption, or energy accommodation,

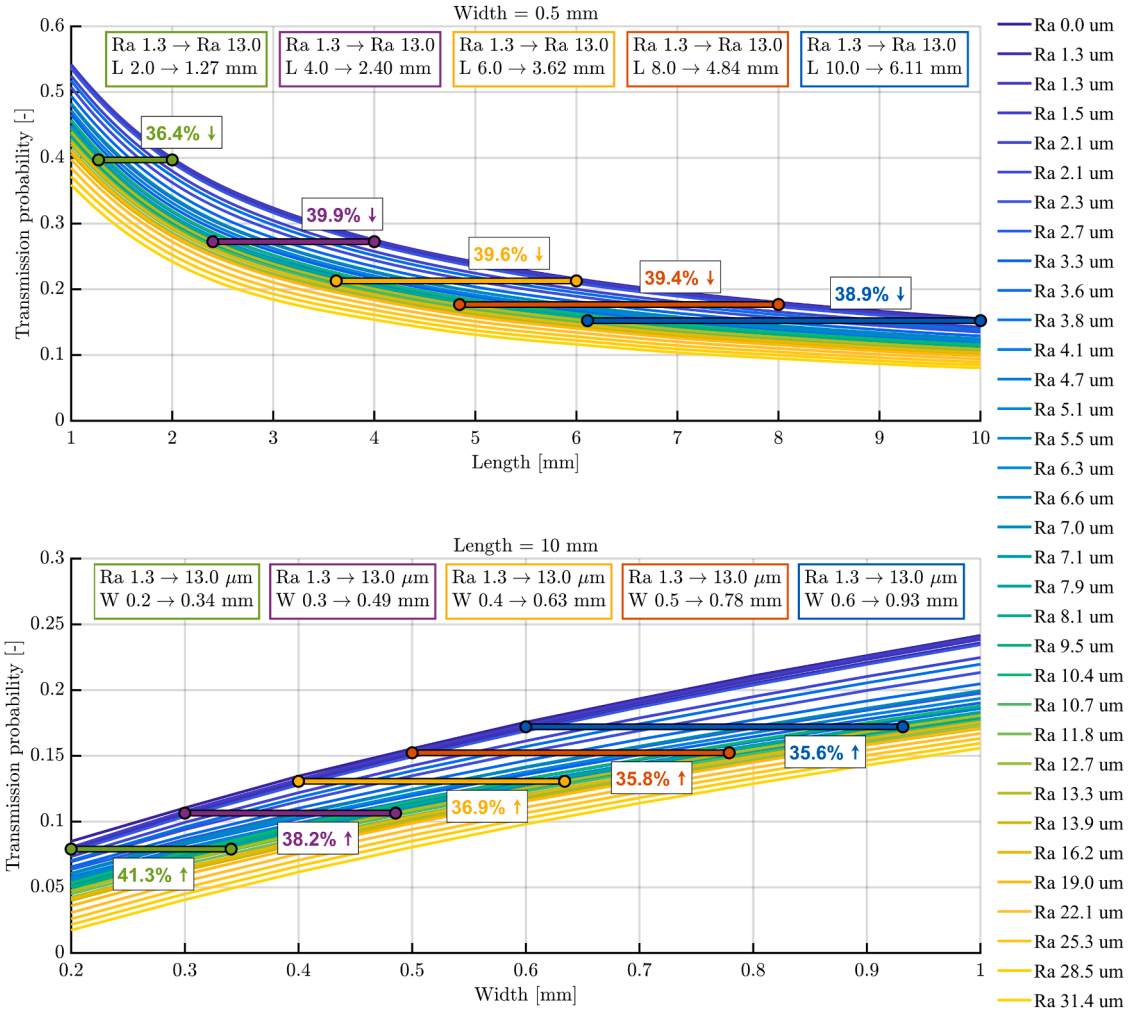

Fig. 12. Design trade-offs enabling seal length reduction or gap widening via increased surface roughness at constant transmission probability.

which may become significant in high-vacuum or reactive environments and could affect the scattering dynamics of molecules [26,47,48].

Finally, as a simulation-based fitted model, its predictive accuracy is constrained by the parameter space explored during its development. Application beyond the validated spectral and geometric ranges may introduce error, and caution is warranted when generalizing to untested conditions. These limitations suggest directions for future refinement, including incorporation of experimental surface data, extension to 3D geometries, and consideration of advanced surface descriptors and thermophysical effects.

5. Conclusion

This study systematically investigates the influence of surface roughness on molecular flow through two-dimensional (2D) labyrinth seals under ultra-high vacuum conditions. By integrating synthetic rough surface profile generation with molecular flow simulations and correction model development, it reveals a clear and consistent relationship between arithmetic mean roughness (*Ra*) and the transmission probability (*TP*) of evaporated lubricant molecules. These findings provide valuable insights for predicting evaporative mass loss and optimizing seal performance.

The results demonstrate a strong inverse correlation between surface roughness and transmission probability, characterized by a nonlinear, saturating decline – most pronounced at lower roughness levels (up to approximately $Ra = 6.0$ μm). Geometric parameters such as channel length and width significantly modulate this effect, with narrower and longer seals intensifying flow resistance due to increased molecule-wall interactions. To generalize these observations, a second-order polynomial correction model based on *Ra* was developed (see Eq.(11)), offering reliable *TP* predictions across a range of seal configurations. providing reliable TP predictions across diverse seal configurations. The model exhibited strong agreement with experimental data, maintaining prediction errors within 5.1 % (see Table 5).

Importantly, the study reveals that increasing surface roughness by an order of magnitude enables either a reduction in labyrinth seal channel length or an increase in gap width by approximately 35–40 %, while maintaining the same transmission probability (see Fig. 12). This insight highlights the potential of controlled surface texturing to improve design flexibility by allowing more compact or manufacturable seal geometries without compromising molecular flow performance.

Key outcomes of this study are:

- Surface roughness impedes molecular flow, with increasing *Ra* leading to decreased transmission probability.
- The effect of roughness is nonlinear, showing greatest sensitivity up to $Ra \approx 6.0$ μm and saturating at higher levels.
- Seal geometry (length and width) strongly influences the impact of roughness, particularly in narrow and elongated configurations.
- A second-order correction model based on *Ra* enables accurate, simplified *TP* predictions across various geometries.
- The model's predictions show strong agreement with experimental results, confirming its practical utility in optimizing labyrinth seals for vacuum applications.
- Controlled surface roughness can be leveraged as a design parameter to reduce seal length or increase gap width by up to 40 %, enhancing compactness and manufacturability without loss of performance.

Declaration of generative AI and AI-assisted technologies in the manuscript preparation process

During the preparation of this work, the author used ChatGPT (OpenAI) for grammar correction and stylistic improvements. After using this tool, the author carefully reviewed and edited the content to ensure accuracy and takes full responsibility for the final version of the manuscript.

Data availability statement

The data supporting the findings of this study are openly available on [Zenodo.org] at [https://doi.org/10.5281/zenodo.15649645], reference number [15,649,645].

CRediT authorship contribution statement

Josef Pouzar: Conceptualization, Data curation, Formal analysis, Funding acquisition, Investigation, Methodology, Project administration, Software, Validation, Visualization, Writing – original draft. **David Kostal:** Conceptualization, Supervision, Writing – review & editing. **Lars-Göran Westerberg:** Conceptualization, Supervision, Writing – review & editing. **Erik Nyberg:** Conceptualization, Methodology, Writing – review & editing. **Tomas Polacek:** Methodology, Validation, Writing – original draft. **Karel Jurik:** Data curation, Software, Writing – review & editing. **Ivan Krupka:** Funding acquisition, Resources, Supervision.

Declaration of competing interest

The authors declare the following financial interests/personal relationships which may be considered as potential competing interests:

Josef Pouzar reports financial support was provided by European Space Agency. Ivan Krupka reports financial support was provided by European Union. If there are other authors, they declare that they have no known competing financial interests or personal relationships that could have appeared to influence the work reported in this paper.

Acknowledgment

This work was supported by the activity "Effect of local geometrical changes and polarization of labyrinth seal surfaces on the evaporation rate of liquid lubricants in space applications", funded as contract Nr. 4000139889 by the European Space Agency; and by the project "Mechanical Engineering of Biological and Bio-inspired Systems", funded as project No CZ.02.01.01/00/22_008/0004634 by Programme Johannes Amos Comenius, call Excellent Research.

Data availability

https://doi.org/10.5281/zenodo.15649645 (The data supporting the findings of this study are openly available on [Zenodo.org] at [], reference number [15,649,645].)

References

[1] S. Krishnan, S.-H. Lee, H.-Y. Hsu, G. Konchady, Lubrication of attitude control systems, in: Advances in Spacecraft Technologies, InTech, 2011. https://doi.org/10.5772/13354.
[2] ESTL, Evaporation Lives of Space Oils, ESA-ESTL-TM-0162 01, 2019. https://llviewersg3a.com/webviewer.php?doc=316948. accessed June 14, 2024.
[3] J. Pouzar, D. Kostal, P. Sperka, I. Krupka, M. Hartl, Experimental study of space lubricant evaporation in a high vacuum environment, Vacuum. 219 (2024) 112758, https://doi.org/10.1016/j.vacuum.2023.112758.
[4] E.W. Roberts, M. Eiden, Space Tribology Handbook, 5th ed., ESR Technology Ltd, 2013. https://llviewersg3a.com/webviewer.php?doc=308770. accessed June 14, 2024.
[5] J. Pouzar, D. Kostal, L.-G. Westerberg, E. Nyberg, I. Krupka, Labyrinth seal design for space applications, Vacuum. 232 (2025) 113882, https://doi.org/10.1016/j.vacuum.2024.113882.
[6] M.N. Gardos, Labyrinth sealing of aerospace mechanisms—theory and practice, A S L E Trans. 17 (1974) 237–250, https://doi.org/10.1080/05698197408981462.
[7] M.J. Anderson, S. Freeman, E.W. Roberts, in: R.~A. Harris (Ed.), Evaporative Losses of Vacuum-Compatible Oils Through Labyrinth Seals, ESMATS, 2003, pp. 255–270. https://www.esmats.eu/esmatspapers/pastpapers/pdfs/2003/anderson.pdf. accessed June 14, 2024.
[8] A. Rowntree, ESTL-TM-238 - a review of oil loss models for labyrinth seals and filters for space applications. https://llviewersg3a.com/webviewer.php?doc=316948, 2000 accessed September 6, 2025.

[9] E.W. Roberts, Space tribology: its role in spacecraft mechanisms, J. Phys. D. Appl. Phys. 45 (2012) 503001, https://doi.org/10.1088/0022-3727/45/50/503001.
[10] M. Buttery, S. Lewis, A. Kent, R. Bingley, M. Cropper, Long-term storage considerations for spacecraft lubricants, Lubricants. 8 (2020) 32, https://doi.org/10.3390/lubricants8030032.
[11] T. Tondu, E. Vanhove, J.F. Roussel, D. Faye, Mixture effects in contaminant reemission, J. Spacecr. Rockets. 53 (2016) 1172–1177, https://doi.org/10.2514/1.A33507.
[12] P. Kadoski Tadeusz, Wojdyna, liquid lubricants for space engineering and methods for their testing, J. KONES Powertrain Transp. 18 (2011). https://www.researchgate.net/publication/267767121_Liquid_lubricants_for_space_engineering_and_methods_for_their_testing.
[13] A. Suliga, O. Ergincan, R. Rampini, Modeling of spacecraft outgassed contamination levels by thermogravimetric analysis, J. Spacecr. Rockets. 58 (2021) 1010–1016, https://doi.org/10.2514/1.A35020.
[14] M. Hasegawa, A. Seireg, R.A. Lindberg, Surface roughness model for turning, Tribol. Int. 9 (1976) 285–289, https://doi.org/10.1016/0301-679X(76)90019-0.
[15] K. Palová, T. Kelemenová, M. Kelemen, Measuring procedures for evaluating the surface roughness of machined parts, Appl. Sci. 13 (2023) 9385, https://doi.org/10.3390/app13169385.
[16] H. Puga, J. Grilo, V.H. Carneiro, Ultrasonic assisted turning of Al alloys: influence of material processing to improve surface roughness, Surfaces 2 (2019) 326–335, https://doi.org/10.3390/surfaces2020024.
[17] S.J. Zhang, S. To, S.J. Wang, Z.W. Zhu, A review of surface roughness generation in ultra-precision machining, Int. J. Mach. Tools. Manuf. 91 (2015) 76–95, https://doi.org/10.1016/j.ijmachtools.2015.02.001.
[18] C. Felho, G. Varga, Theoretical roughness modeling of hard turned surfaces considering tool wear, Machines 10 (2022) 188, https://doi.org/10.3390/machines10030188.
[19] K.J. Stout, T.G. King, D.J. Whitehouse, Analytical techniques in surface topography and their application to a running-in experiment, Wear. 43 (1977) 99–115, https://doi.org/10.1016/0043-1648(77)90046-1.
[20] F. Ticconi, L. Pulvirenti, N. Pierdicc, Models for Scattering from Rough Surfaces, Electromagnetic Waves, InTech, 2011, https://doi.org/10.5772/19318.
[21] Q. Dai, W. Huang, X. Wang, Surface roughness and orientation effects on the thermo-capillary migration of a droplet of paraffin oil, Exp. Therm. Fluid. Sci. 57 (2014) 200–206, https://doi.org/10.1016/j.expthermflusci.2014.04.023.
[22] R. Kersevan, Analytical and numerical tools for vacuum systems, Vac. Accel. (2007) 28, https://doi.org/10.5170/CERN-2007-003.285.
[23] M. Shams, M.H. Khadem, S. Hossainpour, Direct simulation of roughness effects on rarefied and compressible flow at slip flow regime, Int. Commun. Heat Mass Transf. 36 (2009) 88–95, https://doi.org/10.1016/j.icheatmasstransfer.2008.08.018.
[24] Y. Ji, K. Yuan, J.N. Chung, Numerical simulation of wall roughness on gaseous flow and heat transfer in a microchannel, Int. J. Heat. Mass Transf. 49 (2006) 1329–1339, https://doi.org/10.1016/j.ijheatmasstransfer.2005.10.011.
[25] H. Sun, M. Faghri, Effect of surface roughness on nitrogen flow in a microchannel using the direct simulation Monte Carlo method, Numeri. Heat. Transf. a Appl. 43 (2003) 1–8, https://doi.org/10.1080/10407780307302.
[26] O.B. Malyshev, Vacuum in Particle Accelerators, Wiley, 2019, https://doi.org/10.1002/9783527809134.
[27] B.T. Porodnov, P.E. Suetin, S.F. Borisov, V.D. Akinshin, Experimental investigation of rarefied gas flow in different channels, J. Fluid. Mech. 64 (1974) 417–438, https://doi.org/10.1017/S0022112074002485.
[28] COMSOL Multiphysics® v. 6.2. COMSOL AB, Stockholm, Sweden., (n.d.). www.comsol.com (accessed February 27, 2024).
[29] COMSOL, COMSOL Multiphysics | Molecular Flow Module. https://www.comsol.com/molecular-flow-module, 2023.
[30] N. Morrison, Introduction to Fourier Analysis, John Wiley & Sons, 1994.
[31] E.M. Stein, R. Shakarchi, Fourier analysis: An Introduction, Princeton University Press, 2003.
[32] B. Sjodin, How to Generate Random Surfaces in COMSOL Multiphysics®, COMSOL, 2017. https://www.comsol.com/blogs/how-to-generate-random-surfaces-in-comsol-multiphysics. accessed May 26, 2025.
[33] M.F. Barnsley, R.L. Devaney, B.B. Mandelbrot, H.-O. Peitgen, D. Saupe, R.F. Voss, The Science of Fractal Images, Springer New York, New York, NY, 1988, https://doi.org/10.1007/978-1-4612-3784-6.
[34] M.N. Goodhand, K. Walton, L. Blunt, H.W. Lung, R.J. Miller, R. Marsden, The limitations of "Ra" to describe surface roughness. Volume 5C: Heat Transfer, American Society of Mechanical Engineers, 2015, https://doi.org/10.1115/GT2015-43329.
[35] Q.J. Wang, Y.-W. Chung (Eds.), Encyclopedia of Tribology, Springer US, Boston, MA, 2013, https://doi.org/10.1007/978-0-387-92897-5.
[36] B.N.J. Persson, On the use of surface roughness parameters, Tribol. Lett. 71 (2023) 29, https://doi.org/10.1007/s11249-023-01700-z.
[37] M. Piska, J. Metelkova, On the influence of surface roughness on molecular flow and geometric compensation in vacuum labyrinth seals, MM Sci. J. 2014 (2014) 476–480, https://doi.org/10.17973/MMSJ.2014_06_201408.
[38] ISO 21920-2:2021 Geometrical product specifications (GPS) — Surface texture: profile part 2: terms, definitions and surface texture parameters, 2021.
[39] ISO 25178-2:2021 Geometrical product specifications (GPS) — Surface texture: areal part 2: terms, definitions and surface texture parameters, 2021.
[40] G.P. Petropoulos, A.A. Torrance, C.N. Pandazaras, Abbott curves characteristics of turned surfaces, Int. J. Mach. Tools. Manuf. 43 (2003) 237–243, https://doi.org/10.1016/S0890-6955(02)00240-7.
[41] P. He, S. Lu, Y. Wang, R. Li, F. Li, Analysis of the best roughness surface based on the bearing area curve theory, Proc. Inst. Mech. Eng. J: J. Eng. Tribol. 236 (2022) 527–540, https://doi.org/10.1177/13506501211018937.
[42] A. Doniavi, Empirical modeling of surface roughness in turning process of 1060 steel using factorial design methodology, J. Appl. Sci. 7 (2007) 2509–2513, https://doi.org/10.3923/jas.2007.2509.2513.
[43] D. Vukelic, K. Simunovic, Z. Kanovic, T. Saric, K. Doroslovacki, M. Prica, G. Simunovic, Modelling surface roughness in finish turning as a function of cutting tool geometry using the response surface method, gaussian process regression and decision tree regression, Adv. Prod. Eng. Manag. 17 (2022) 367–380, https://doi.org/10.14743/apem2022.3.442.
[44] O. Sazhin, The effect of surface roughness on internal free molecular gas flow, Vacuum. 159 (2019) 287–292, https://doi.org/10.1016/j.vacuum.2018.09.031.
[45] K. Jousten, W.H. Vakuumtechnik, Vieweg+Teubner Verlag, Wiesbaden, 2004, https://doi.org/10.1007/978-3-322-96971-2.
[46] The Vacuum Technology Book, II, Pfeiffer Vacuum, 2013. | Volume.
[47] M. Gleirscher, A. Wolfberger, S. Schlögl, M. Hołyńska, A. Hausberger, Accelerated thermo-catalytic degradation of perfluoropolyether (PFPE) lubricants for space applications, Lubricants. 11 (2023) 81, https://doi.org/10.3390/lubricants11020081.
[48] M. Hołyńska, R.-C. Sarah, E. Orcun, B. Bruno, A. Claudia, R. Riccardo, Lessons learnt from lubricants' Testing at Estec Materials' laboratories. https://www.esmats.eu/esmatspapers/pastpapers/pdfs/2021/holynska.pdf, 2021.